

ALMA Observations of the Galactic Center: SiO Outflows and High Mass Star Formation near Sgr A*

F. Yusef-Zadeh¹, M. Royster¹, M. Wardle², R. Arendt³, H. Bushouse⁴, D. C. Lis⁵, M. W. Pound⁶, D. A. Roberts¹, B. Whitney⁷ and A. Wootten⁸

¹*Department of Physics and Astronomy and Center for Interdisciplinary Research in Astronomy, Northwestern University, Evanston, IL 60208*

²*Department of Physics and Astronomy, and Research Centre for Astronomy, Astrophysics & Astrophotonics, Macquarie University, Sydney NSW 2109, Australia*

³*CREST/UMBC/NASA GSFC, Code 665, Greenbelt, MD 20771*

⁴*Space Telescope Science Institute, 3700 San Martin Drive, Baltimore, MD 21218*

⁵*California Institute of Technology, MC 320-47, Pasadena, CA 91125*

⁶*University of Maryland, Department of Astronomy, MD 20742*

⁷*Space Science Institute, 4750 Walnut Street, Suite 205, Boulder, CO 80301*

⁸*National Radio Astronomy Observatory, Charlottesville, VA 22903*

ABSTRACT

ALMA observations of the Galactic center with spatial resolution $2.61'' \times 0.97''$ resulted in the detection of 11 SiO (5-4) clumps of molecular gas within 0.6pc (15'') of Sgr A*, interior to the 2-pc circumnuclear molecular ring. The three SiO (5-4) clumps closest to Sgr A* show the largest central velocities, $\sim 150 \text{ km s}^{-1}$, and broadest asymmetric linewidths with full width zero intensity (FWZI) $\sim 110 - 147 \text{ km s}^{-1}$. The remaining clumps, distributed mainly to the NE of the ionized mini-spiral, have narrow FWZI ($\sim 18 - 56 \text{ km s}^{-1}$). Using CARMA SiO (2-1) data, LVG modeling of the the SiO line ratios for the broad velocity clumps, constrains the column density $N(\text{SiO}) \sim 10^{14} \text{ cm}^{-2}$, and the H_2 gas density $n_{\text{H}_2} = (3-9) \times 10^5 \text{ cm}^{-3}$ for an assumed kinetic temperature 100-200K. The SiO clumps are interpreted as highly embedded protostellar outflows, signifying an early stage of massive star formation near Sgr A* in the last $10^4 - 10^5$ years. Support for this interpretation is provided by the SiO (5-4) line luminosities and velocity widths which lie in the range measured for protostellar outflows in star forming regions in the Galaxy. Furthermore, SED modeling of stellar sources shows two

YSO candidates near SiO clumps, supporting in-situ star formation near Sgr A*. We discuss the nature of star formation where the gravitational potential of the black hole dominates. In particular, we suggest that external radiative pressure exerted on self-shielded molecular clouds enhances the gas density, before the gas cloud become gravitationally unstable near Sgr A*. Alternatively, collisions between clumps in the ring may trigger gravitational collapse.

Subject headings: Galaxy: center - clouds - ISM: general - ISM - radio continuum
- stars: protostars

1. Introduction

The compact radio source Sgr A* located at the very dynamical center of our galaxy coincides with a $4 \times 10^6 M_{\odot}$ black hole (Ghez *et al.* 2008; Gillessen *et al.* 2009). Star formation near Sgr A* is forbidden, unless the gas density is large enough for self-gravity to overcome the strong tidal shear of the black hole. One viable mechanism is cloud capture to form a massive and dense gaseous disk around the black hole. The disk becomes gravitationally unstable, creating a new generation of stars (e.g., Levin and Beloborodov 2003; Nayakshin *et al.* 2007; Paumard *et al.* 2006; Lu *et al.* 2009; Mapelli *et al.* 2012; Wardle & Yusef-Zadeh 2008; Bonnell & Rice 2008; Alig *et al.* 2012). This formation scenario has been applied to disk-like distribution of young stars on a scale of 0.03-0.3 pc, to the 2-5pc circumnuclear molecular ring (CND or CNR) orbiting Sgr A* as well as to AGNs with megamaser disks (Wardle & Yusef-Zadeh 2008; 2012). The Galactic center provides an opportunity for testing models of stellar birth with far reaching implications on the nature of star formation in the nuclei of galaxies hosting massive black holes.

Because the age of the stellar disk orbiting Sgr A* is several million years, it is not possible to identify signatures of early phases of star formation such as maser activity near the black hole. However, a number of recent studies suggest infrared excess sources in the N arm, as well as young stellar object (YSO) candidates in IRS 13N within a projected distance of 0.12 pc (3'') from Sgr A* (e.g., Viehmann *et al.* 2006; Eckart *et al.* 2012; Nishiyama and Schödel 2013). These measurements imply that star formation has taken place within $\sim 10^5$ years. On a larger scale of $50'' - 100''$, or projected distance of 2-4 pc (assuming that the distance to the Galactic center is 8.5 kpc), the molecular ring (Jackson *et al.* 1993; Montero-Castano *et al.* 2009, Martin *et al.* 2012) that encircles Sgr A* with a rotational velocity of $\sim 100 \text{ km s}^{-1}$ shows signatures of massive star formation activity within the last $\sim 10^4 - 10^5$ years (Yusef-Zadeh *et al.* 2008). Here, we present the earliest signatures of on-going star formation on a scale of about $11''$ (0.44 pc) from Sgr A*: the presence of

SiO (5-4) line emission around the interior of the molecular ring. The SiO molecule is an *excellent* tracer of protostellar outflows and is shock excited, since silicon is removed from dust grains, significantly increasing gas-phase abundance.

2. Observations and Data Reduction

ALMA: The data were obtained through the ALMA Science Verification process on June 26, 2011. Utilizing only twelve of the 12 m antennas, the observations consisted of a 7-point mosaic at the position of Sgr A*: $(\alpha, \delta) = 17^h 45^m 40^s.04, -29^\circ 0' 28''.12$. Titan was initially used as the flux calibrator and 3C279 as the initial bandpass and phase calibrator. NRAO 530 was observed periodically to correct for any changes in phase and amplitude as a function of time. Four basebands of total width 1.875 GHz were used with the high spectral resolution, which contained 3840 channels each. The spectral windows were centered at roughly: 216.2 GHz, 218.0 GHz, 231.9 GHz, and 233.7 GHz. The SiO (5-4) line emission is centered at 217.105 GHz. The editing and calibration of the data was carried out by the Science Verification team in CASA. The imaging was completed by modifying the supplied imaging script. SiO 5-4 fell at the intersection of the first two basebands at 216.2 GHz and 218.0 GHz. As a result, care was taken to note any changes in amplitude and phase at the edge channels in combining the two windows. A linear continuum was fitted and subtracted from the line-free channels before CLEANing. The data was averaged by a factor of five to achieve a spectral resolution of 3.371 km s^{-1} (2.441 MHz) using the raw binning of 0.674 km s^{-1} (0.488 MHz). To avoid confusion with nearby lines, we studied velocity structures within 440 km s^{-1} spatial resolutions of $2.61'' \times 0.97''$.

CARMA: The SiO (2-1) line data were taken with the Combined Array for Research in Millimeter-wave Astronomy (CARMA) during the 2009 and 2010 observing seasons in the D and C array configurations. The array consisted of six 10.4m antennas and nine 6.1m antennas and the maps were made on a 127-point hexagonal mosaic, Nyquist-sampling the 10.4m antenna primary beam. The spatial resolution and spectral resolutions of the final maps are $8.87'' \times 4.56''$ and 6.74 km s^{-1} , respectively.

3. Results and Discussion

Figure 1a shows a composite 3.6 cm continuum image of the three arms of the mini-spiral (Sgr A West) surrounded by the CNR as traced by HCN line emission (Christopher *et al.* 2005). The inner $1'$ (2.4pc) of the CNR, as observed with ALMA, shows a large concentration

of molecular clumps in the SiO (5-4) line emission. The distribution of molecular and ionized gas orbiting Sgr A* is generally described as a central cavity that consists of ionized gas of Sgr A West coupled to the surrounding molecular ring (e.g. Roberts and Goss 1993; Serabyn and Lacy 1985). A string of SiO clumps is found in the region between the N and E arms of Sgr A West. A close up view of these clumps is shown in Figure 1b. What is most interesting is the presence of SiO clumps in the interior of the ring, which is expected to be dominated by the central cavity of ionized gas and atomic gas traced by [OI] emission, devoid of any molecular gas. Figure 1b also shows two clumps (green), with velocities $v_r \sim 136$ to 160 km s^{-1} , and FWHM linewidths 47 to 55 km s^{-1} . These ALMA clumps, 1 and 11, are located about $7''$ NE and $11''$ SW of Sgr A*, respectively, and do not follow the kinematics of the molecular ring orbiting Sgr A*. Figure 1c shows the positions of these highly redshifted velocity clumps on a $3.6\mu\text{m}$ image taken with the VLT. Clumps 1 and 2 lie $\sim 2''$ west of IRS 1W, a mass-losing W-R star with a bow shock structure (Tanner *et al.* 2003).

To illustrate the kinematics of SiO (5-4) molecular clumps, the spectra of broadest velocity clumps are shown in Figure 1d whereas the spectra of 8 clumps with narrow linewidths within the ring are shown in Figure 2 where the distribution of SiO (5-4) peak line emission is shown. Columns 1 to 7 of Table 1 list the source numbers, coordinates, intensity of the peak emission, Gaussian fitted central velocity, FWHM linewidths, and FWZI of the 11 sources labeled in Figure 2. FWZI linewidths are listed because many sources show velocity profiles with blue-shifted wings (e.g., clumps 1, 2, 11). Clumps 4 to 8 run parallel to the eastern edge of the N arm of ionized gas showing typical linewidths between 11 and 21 km s^{-1} and peak radial velocities that decrease from 37.8 km s^{-1} at Clump 8 to 7.4 km s^{-1} at Clump 4. The trend in radial velocity change in molecular clumps is consistent with the trend in the kinematics of ionized gas of the N arm (e.g., Zhao *et al.* 2011). However, the central velocities of ionized in the N arm are $\sim 100 \text{ km s}^{-1}$ and decrease to 0 km s^{-1} as the ionized gas approaches closer to Sgr A* (e.g., Roberts and Goss 1993; Jackson *et al.* 1993; Zhao *et al.* 2011). The kinematics of SiO (5-4) is dissimilar to that of the ionized gas of the N arm and the "tongue" of neutral [OI] gas. The spatial and velocity distributions of SiO (5-4) suggest a clumpy and dense molecular cloud lying in the interior of the molecular ring.

Clumps 1, 2 and 3 defy the kinematical trend of the N arm: they display highly redshifted ($< 160 \text{ km s}^{-1}$) and blue-shifted velocity (-28 km s^{-1}) components and lie adjacent to the ionized gas of the N arm, but with dissimilar velocities. Figure 3a shows contours of highly red-shifted SiO (5-4) line emission from Clumps 1 and 2 superimposed on a 3cm continuum image of the N arm. The SiO line emission from Clump 1 appears to be elongated to the NE with non-Gaussian velocity profiles having blue-shifted wings. Another morphological structure of the N arm is the wavy structure along the direction of the flow

(Yusef-Zadeh and Wardle 1993; Zhao *et al.* 2012). Figure 3b shows contours of SiO (5-4) emission from Clump 3 superimposed on a 3cm continuum image. The spectrum of Clump 3 that lies adjacent to the wavy structure shows a radial velocity peaking at $v \sim -28 \text{ km s}^{-1}$ and linewidth of $v_{\text{FWHM}} \sim 27 \text{ km s}^{-1}$ with a broad blue-shifted wing extending to -100 km s^{-1} . This radial velocity is inconsistent with circular motion orbiting Sgr A*. Several radio dark clouds (Yusef-Zadeh 2012) lie to the east of the N arm in Figures 3a,b where Clumps 1, 2 and 3 lie. These dark features trace molecular gas and are embedded in the ionized gas of the N arm. Although the morphology of thermal radio emission at the location of Clumps 1 and 3 suggests that the flow of ionized gas is distorted as a result of its interactions with molecular clumps, the kinematics of the molecular and ionized gas are inconsistent with the interaction picture.

Protostellar Outflows: To examine the physical properties of SiO clumps, we focus on the SiO (5-4) and (2-1) line profiles, as shown in Figure 3c, with peak line emission $T_{\text{MB}} \sim 0.95$ and 0.65 K , for Clump 1 and $T_{\text{MB}} \sim 1.1$ and 1 K , for Clump 11 at center velocity of ~ 147 and $\sim 136 \text{ km s}^{-1}$, respectively. The similarity of SiO (5-4) and (2-1) line profiles toward Clumps 1 and 11 is a classic signature of one-sided molecular outflows in star forming regions (e.g., Plambeck & Menten 1990). We used the Large Velocity Gradient (LVG) model to constrain the density and column density. The result of this analysis is shown in Figure 3d. Assuming that the beam filling factor is 0.5, thus, 1 mJy is equivalent to $T_{\text{MB}} = 20.5$ and 7.96 mK for SiO (5-4) and SiO (2-1) data, respectively, the gas density of hydrogen nuclei is constrained to $n_{\text{H}_2} \sim (3 - 9) \times 10^5 \text{ cm}^{-3}$ within a temperature range 100-200K. The synthesized beam is highly elongated in one direction, thus we chose a beam filling factor of 0.5. Multi-transition CO and NH₃ studies of the inner 2pc derive kinetic temperature 100-200K and warm gas in the interior of the molecular ring (Bradford *et al.* 2005; Herrnstein and Ho 2005). $N(\text{SiO})/\Delta v \sim 1.7 - 2.4 \times 10^{12} \text{ cm}^{-2} \text{ km s}^{-1}$ is better constrained than the gas density, as shown in the bottom panel of Figure 3d. The column densities of SiO for Clumps 1 and 11 are estimated to be $N(\text{SiO}) \sim 8.6 \times 10^{13}$ and $\sim 1.3 \times 10^{14} \text{ cm}^{-2}$, respectively. The total mass of molecular gas is estimated to be $\sim 0.2 M_{\odot}$ using clump radius 0.03 pc ($0.79''$) for an unresolved sources and $n_{\text{H}_2} = 10^6 \text{ cm}^{-3}$. This corresponds to a column density of $1.8 \times 10^{23} \text{ cm}^{-2}$ and SiO abundance of 5.6×10^{-10} which is clearly much higher than is expected in quiescent molecular clouds. Using the size and the FWHM velocity widths, the velocity gradient is estimated to be 833 and $165 \text{ km s}^{-1} \text{ pc}^{-1}$ for clumps with broad ($\sim 50 \text{ km s}^{-1}$) and narrow ($\sim 10 \text{ km s}^{-1}$) linewidths respectively. These imply that the clumps can not be bound by self-gravity because the collapse time scale is 12-58 times longer than the dynamical time scales $t_{\text{dyn}} \sim (0.3 - 1.5) \times 10^3 \text{ years}$, thus are likely to be outflows from YSOs. The blue-shifted velocity wings and non-circular radial velocities in orbital motion about Sgr A* is also consistent with SiO outflows in which the approaching

side of the outflow has burst through the edge of a molecular cloud.

One strong piece of evidence that the SiO sources are YSO outflows is that the luminosities and velocity widths lie in the range detected from protostellar outflows in star forming regions. Figure 4 compares the SiO (5-4) luminosity and FWZI for the detected sources inside the molecular ring, to those for samples of low-mass and high-mass YSOs (Gibb *et al.* 2004 and 2007). The SiO 5-4 luminosities for the low-mass and high-mass YSO samples tabulated in Gibb *et al.* (2004, 2007) have been corrected by multiplying by 1500 and 170, respectively (A. Gibb, private communication). All three samples show the same wide range of velocity widths, and the luminosities of SiO clumps interior to the molecular ring fall in between those of the low-mass and high-mass YSOs.

What sources drive the outflows? We identified two new YSO candidates in the N arm near Clumps 1 and 3. Figure 3e shows contours of SiO (5-4) emission from Clumps 1 and 5 superimposed on a ratio map of L ($3.6\mu\text{m}$) to K ($1.6\mu\text{m}$) band images from VLT observations. The ratio map shows the dusty environment of the N arm. The crosses coincide with the positions of YSO candidates with the positional uncertainty of $1.18''$ at $8\mu\text{m}$ (Ramirez *et al.* 2008). The SEDs of these sources are analyzed by comparing a set of SEDs enhanced by a large grid of YSO models (Whitney *et al.* 2003; Robitaille *et al.* 2007), as Figure 3f shows their fitted SEDs. The source 526311, which is selected from their IR colors, is classified as a Stage I YSO candidate, whereas the red source 526817 is a YSO candidate but its classification is uncertain. These YSO candidates have typical ages of 10^5 years. By fitting the SEDs, we derive masses of 34.3 ± 5.9 and $19.4 \pm 2.5 M_{\odot}$, luminosities $1.8 \pm 0.7 \times 10^5$ and $4.4 \pm 1.5 \times 10^4 L_{\odot}$ and mass-loss rates $5.1 \pm 0.1 \times 10^{-4}$ and $2.5 \pm 0.1 \times 10^{-4} M_{\odot} \text{ yr}^{-1}$ for clumps 1 and 5, respectively. YSO candidate 526817 coincides with the brightest source IRS 10E (Viehmann *et al.* 2006) at the center of Clump 3 whereas the YSO candidate 526817 is an unresolved component of multiple sources in IRS 1. The proximity of massive YSO candidates, SiO (5-4) Clumps near IRS 1 and IRS 10 clusters containing W-R stars, suggest that there is still on-going star formation near these stellar clusters. Similar distribution of massive YSOs, and W-R stars are found in the IRS 13 cluster (Fritz *et al.* 2012; Eckart *et al.* 2012).

Star Formation Mechanism: We have detected the presence of several SiO (5-4) clumps within a pc of Sgr A*. Their SiO (5-4) luminosities, non-Gaussian velocity profiles, large linewidths unbound by self-gravity and dense gas, as traced by dark radio clouds, all point to the conclusion that these clumps are tracing YSOs with protostellar outflows. Thus, our observations reveal earliest stages of massive star formation near Sgr A* on a time scale of $\sim 10^4 - 10^5$ years. Additional support for star formation on a time scales of $\sim 10^5$ years come from SED fitted YSO candidates with infrared excesses on $\sim 10^6$ year timescales, as

well as young stellar disks orbiting Sgr A*, respectively. These suggest that star formation is continuous near Sgr A*.

The mechanism by which star formation can take place in this tidally stressed environment is not well understood. The H₂ density in the molecular ring, $\sim 10^6 - 10^7 \text{ cm}^{-3}$, is well below that needed for self-gravity to overcome the tidal field of the central black hole, i.e. $2 \times 10^8 (r/1\text{pc})^{-3} \text{ cm}^{-3}$. Star formation in this region must therefore be triggered by significant compression of the ambient gas in the ring. Tidal squeezing of an elongated infalling cloud can compress the gas in two dimensions, but the density needs to be increased by two orders of magnitude as the cloud approaches Sgr A*. Here we consider two other possibilities: (i) compression by the intense UV radiation field in the Galactic center, and (ii) clump-clump collisions.

Hot stars in the central parsec produce an intense radiation field with an effective temperature $\sim 3 \times 10^4 \text{ K}$ and a luminosity of order $\sim 10^{7.5} L_{\odot}$ (Lacy et al. 1980; Davidson et al. 1992). The radiation pressure is capable of producing significant compression. Equating the radiation pressure to the thermal pressure of the compressed molecular gas, i.e. $L/(4\pi c D^2) = 1.2 n_{\text{H}_2} kT$, where D is the distance to the center of the hot star distribution, yields $n_{\text{H}_2} \sim 4 \times 10^8 (L/10^{7.5} L_{\odot})(D/0.1\text{pc})^{-2}(T/100\text{K})^{-1} \text{ cm}^{-3}$, comparable to the critical density. It is therefore possible for the pressure associated with irradiation by the UV field to compress a gas clump to the point of gravitational collapse. Note, however, that the clump must be exposed to the radiation field for about 5×10^4 years for the compression to work its way through the entire clump and that much of the momentum may be deposited in a photoevaporative outflow.

Clump-clump collisions are an alternative method for producing SiO emission, either through the destruction of dust grains in large scale shock waves associated with the collision, or via outflows from YSOs formed, because the compression associated with the shock waves triggered star formation. This model, however has difficulty in producing the number of detected sources. Suppose a clump in the interior to the ring has radius r , clump-clump velocity dispersion v and volume filling factor f . Then the number of clumps per unit volume is $n_{cl} = f/(4/3\pi r^3)$, the cross section for almost head-on collisions is $\sigma \sim 2\pi r^2$, and the time scale for a given clump to collide with another is $1/(n_{cl}\sigma v)$. For an ensemble of N clumps, the number of collisions per unit time is $N n_{cl}\sigma v \approx 1.5 \times N f v/r$. The collisional interaction time is approximately $2r/v$, so the number of collisions occurring at any given time is $(N f v/r) \times (2r/v) = 3f N$. For the interior of the molecular ring with a radius of $15''$, a clump size $1.5''$, $f = 10^3/N$ and the number of visible clumps is $3Nf = 11$, thus a population of 60 clumps are needed to produce the number of observed SiO clumps.

In conclusion, ALMA observations show that the interior of the circumnuclear molecular

ring is not completely filled with ionized gas (see the review by Genzel et al. 2010) but is a site of on-going star formation. The linewidths of these clumps are too large to be gravitationally bound, thus suggesting outflows from YSOs. The SiO clumps we found in the Galactic center are highly excited but show properties that are similar to those found in star formation regions. We suggest that the required high gas density is produced by the strong external radiation field from young massive stars compressing the gas, thus inducing star formation or that clump collisions can account for compressing the gas. Future observations will determine the total mass of molecular gas residing inside the ring, will allow estimating the efficiency of star formation within a pc of Sgr A* and will examine if the molecular gas inside the ring is dynamically important in perturbing the dynamics of stars close to Sgr A*.

We thank Stefan Gillessen for providing us with VLT images. This paper makes use of the following ALMA data: ADS/JAO.ALMA#2011.0.00005.SVProject code. ALMA is a partnership of ESO (representing its member states), NSF (USA) and NINS (Japan), together with NRC (Canada) and NSC and ASIAA (Taiwan), in cooperation with the Republic of Chile. The Joint ALMA Observatory is operated by ESO, AUI/NRAO and NAOJ.

REFERENCES

- Alig, C., Burkert, A., Johansson, P. H. & Schartmann, M. 2012, MNRAS 412, 486
- Bonnell, I. A., & Rice, W. K. M. 2008, Science, 321, 1060
- Bradford, C. M., Stacey, G. J., Nikola, T., *et al.* 2005, ApJ, 623, 866
- Christopher, M. H., Scoville, N. Z., Stolovy, S. R., Yun, M. S. 2005, ApJ, 622, 346
- Davidson, JA, Werner, MW, Wu, X *et al.* 1992, ApJ, 387, 189
- Eckart, A., Muzic, K., Yazici, S., Shahzamanian, B. *et al.* 2012, A&A (arXiv1208.1907)
- Genzel, R., Eisenhauer, F., & Gillessen, S. 2010, Reviews of Modern Physics, 82, 3121
- Ghez, A. M., Salim, S., Weinberg, N. N. *et al.* 2008, ApJ, 689, 1044
- Gibb, A. G., Richer, J.S., Chandler, C.J., & Davis, C. J. 2004, ApJ, 603, 198
- Gibb, A. G., Davis, C. J. & Moore, T. J. T. 2007, MNRAS, 382, 1212
- Gillessen, S., Eisenhauer, F., Trippe, S. *et al.* 2009, ApJ, 692, 1075
- Herrnstein, R. M. & Ho, P. T. P. 2005, ApJ, 620, 287

- Jackson, J. M., Geis, N., Genzel, R., Harris, A. I., Madden, S. *et al.* 1993, ApJ, 402, 173
- Lacy, J.H., Townes, CH, Geballe, T. R. *et al.* 1980, ApJ, 241, 132
- Levin, Y. & Beloborodov, A. M. 2003, ApJ, 590, L33
- Lu, J. R., Ghez, A. M., Hornstein, S. D. *et al.* 2009, ApJ, 690, 1463
- Mapelli, M., Hayfield, T., Mayer, L. & Wadsley, J. 2012, ApJ, 749, 168
- Martin, M. Martin-Pintado, J., Montero-Castano, M. *et al.* 2012, A&A, 539, 29
- Montero-Castano, M., Herrnstein, R. M. & Ho, Paul T. P. 2009, ApJ, 695, 1477
- Paumard, T., Genzel, R., Martins, F. *et al.* 2006, ApJ, 643, 1011
- Nayakshin, S., Cuadra, J. & Springel, V. 2007, MNRAS, 379, 21
- Nishiyama, S. & Schödel, R. 2013, A&A, 549, 16
- Plambeck, R. L. & Menten, K. M. 1990, ApJ, 364, 555
- Ramirez, S. V., Arendt, R. G. & Sellgren, K. *et al.* 2008, ApJS, 175, 147
- Roberts, D. A. & Goss, W. M. 1993, ApJS, 86, 133
- Robitaille, T. P., Whitney, B. A., Indebetouw, R. *et al.* 2007, ApJS, 169, 328
- Serabyn, E. & Lacy, J. H. 1985, ApJ, 293, 445
- Tanner, A., Ghez, A. M., Morris, M. R. & Christou, J. C. 2005, ApJ, 624, 742
- Viehmann, T., Eckart, A., Schödel, *et al.* 2006, ApJ, 642, 861
- Wardle, M., & Yusef-Zadeh, F. 2008, ApJ, 683, L37
- Wardle, M., & Yusef-Zadeh, F. 2012, ApJ, 750, L38
- Whitney, B. A. and Wood, K. and Bjorkman, J. E. & Wolff, M. J., 2003, ApJ, 591, 1049
- Yusef-Zadeh, F. 2012, ApJ, 759, 8
- Yusef-Zadeh, F., Braatz, J., Wardle, M., & Roberts, D. 2008, ApJ, 683, L147
- Yusef-Zadeh, F., Hewitt, J. W., Arendt, R. G., Whitney, B., Rieke, G. *et al.* 2009, ApJ, 702, 178

Yusef-Zadeh, F. & Wardle, M. 1993, *ApJ*, 405, 584

Zhao, J.-H., Blundell, R., Moran, J. *et al.* 2010, *ApJ*, 723, 1097

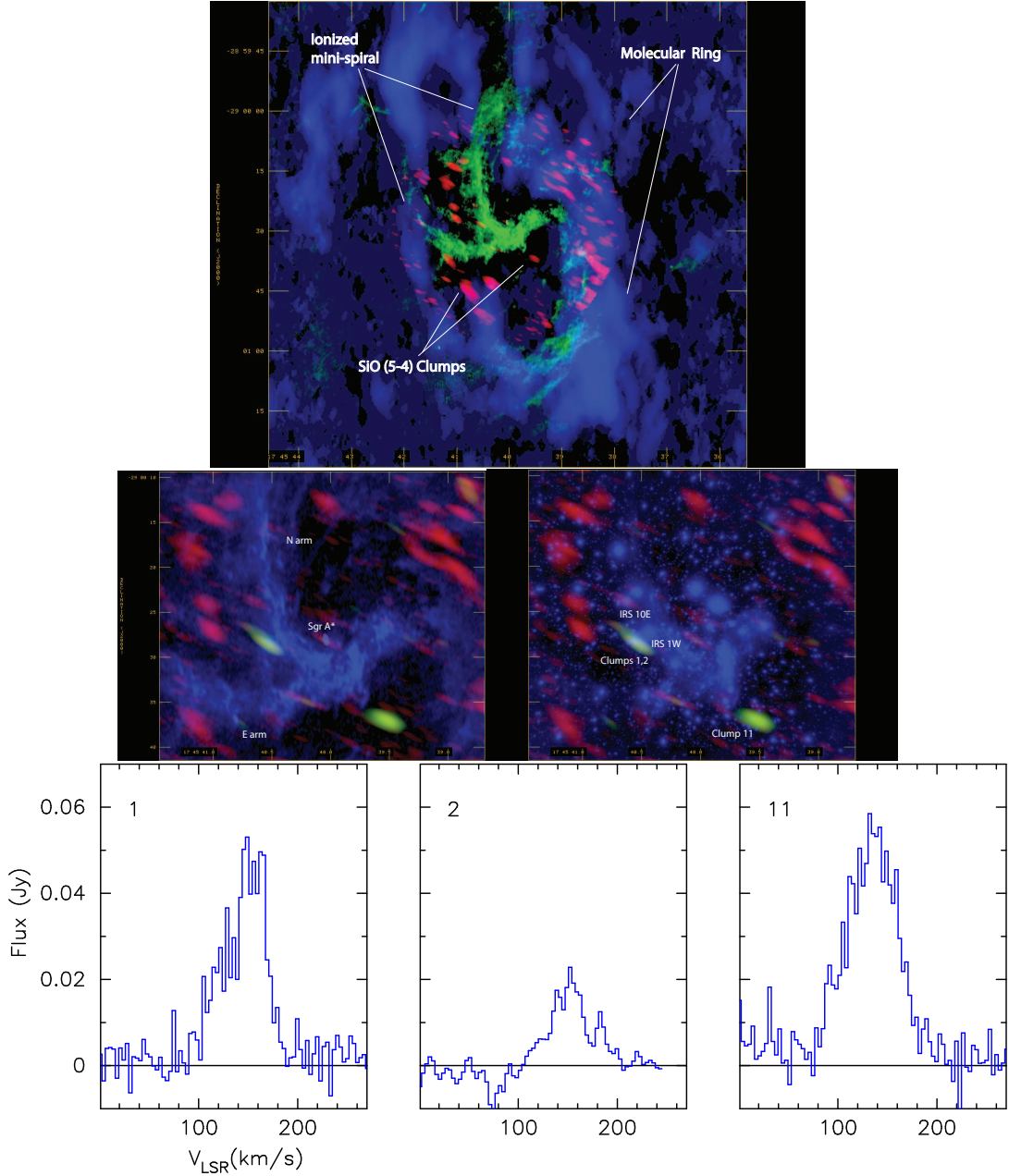


Fig. 1.— (a) A composite image of the inner $2'$ of the Galactic center: 3.6 cm continuum image of Sgr A West (green), HCN (1-0) emission from the molecular ring (blue; Christopher *et al.* 2005) and SiO (5-4) line emission from the central region of the ring (red) (b) The distribution of SiO line emission (red) integrated over velocities $150 < v < 200 \text{ km s}^{-1}$ and superimposed on a 3.6 cm continuum image (blue). The edge of the SiO (5-4) clump distribution is noisier because of shorter integration time and is limited by the size of the region mapped by ALMA. The highest redshifted velocity SiO (5-4) clumps 1 and 11 are shown in green. (c) Similar to (b) except that a $3.6\mu\text{m}$ image taken with the VLT in blue replaces the 3.6 cm image. (d) The spectra of Clumps 1, 2 and 11.

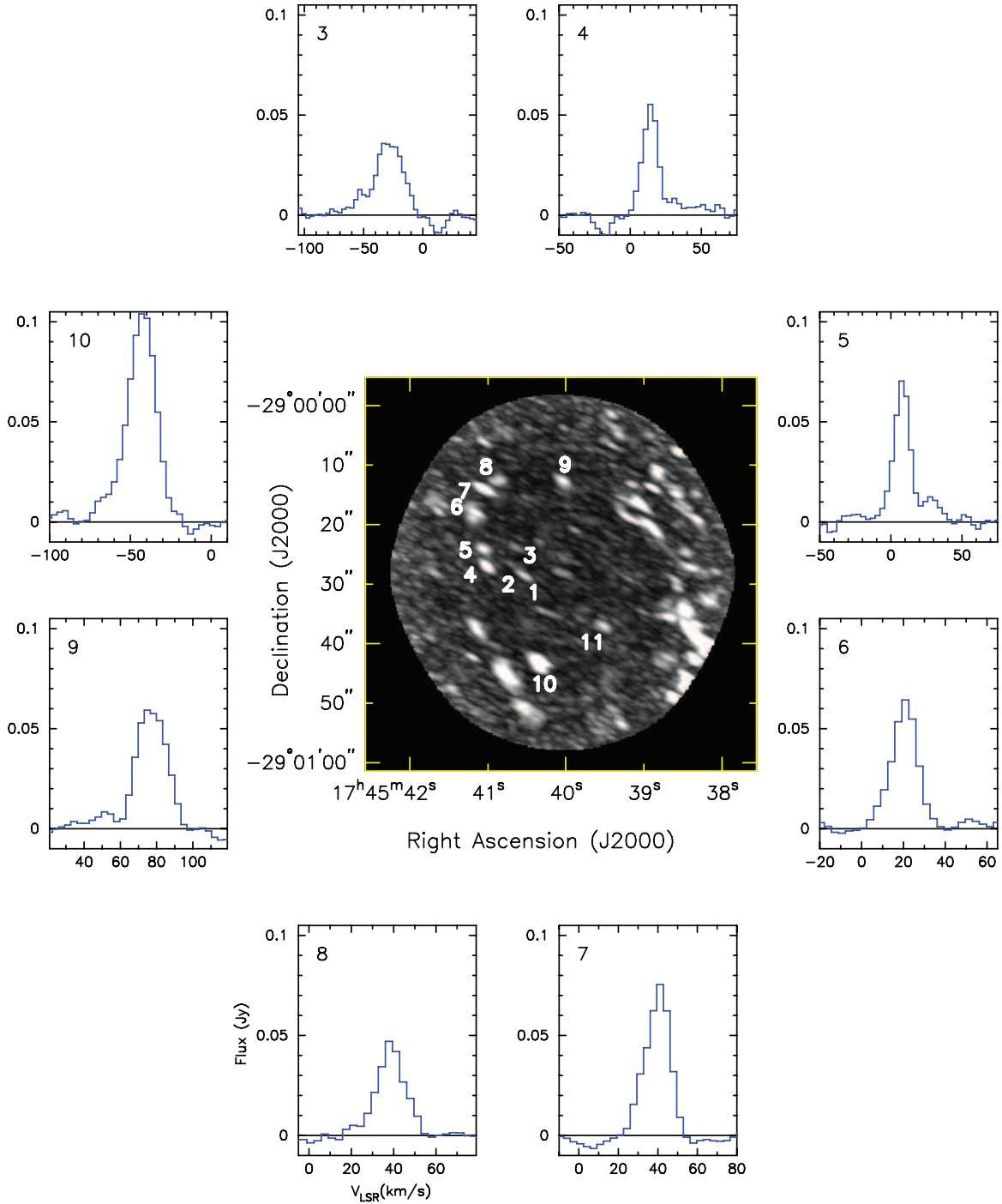


Fig. 2.— A grayscale image constructed from the peak SiO (5-4) line emission between $-191 < v < 213 \text{ km s}^{-1}$. The inset shows the spectra of 8 SiO (5-4) clumps (Jy on Y-axis vs km s^{-1} on the X-axis) within the molecular ring. The positions of labeled spectra are listed in Table 1.

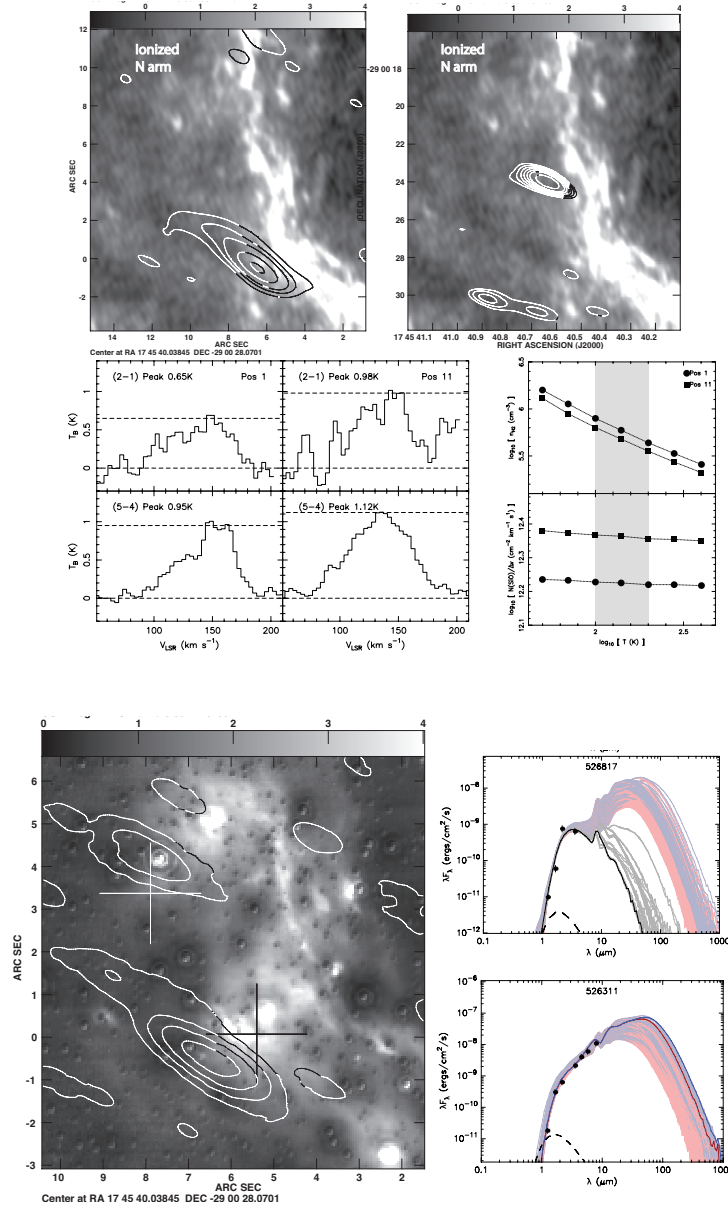


Fig. 3.— (a) Contours of SiO (5-4) line emission from Clumps 1 and 2 integrated between 88 and 188 km s⁻¹ superimposed on a 3cm continuum image. (b) Same as (a) except contours of SiO (5-4) line emission integrated over 0 and -50 km s⁻¹ (c) SiO (5-4) and (2-1) line profiles of Clumps 1 and 11 (labeled as POS 1 and 11). (d) The inferred H₂ density (Top) and N(SiO)/Δv (bottom) as a function of temperature. The band (gray) shows the temperature range of the CNR. (e) Contours of SiO(5-4) emission from Clumps 1 and 3 superimposed on a ratio map of L (3.6μm) to K (1.6 μm) bands. The crosses show the positions of YSO candidates. (f) Fitted SEDs of the two YSO candidates 526311 and 526817 in the vicinity of Clumps 1 and 3, respectively. 526311 and 526817 are designated in the catalog by Ramirez et al. 2008.

Table 1. Gaussian Line Parameters of Fitted SiO Sources

Source	RA (J2000)	DEC (J200)	Peak mJy/beam	Center km s ⁻¹	FWHM km s ⁻¹	FWZI km s ⁻¹
1	17:45:40.51	-29.0.28.78	38.91 ± 2.28	147.81 ± 1.35	47.42 ± 3.29	110 ± 40
2	17:45:40.74	-29.0.26.11	13.92 ± 1.36	159.81 ± 2.60	54.81 ± 6.39	120 ± 41
3	17:45:40.61	-29.0.23.90	35.43 ± 1.84	-27.86 ± 0.69	27.11 ± 1.66	55 ± 19
4	17:45:41.01	-29.0.27.03	77.75 ± 3.17	7.98 ± 0.23	11.52 ± 0.55	25 ± 9
5	17:45:41.06	-29.0.24.09	62.14 ± 3.19	14.28 ± 0.28	11.15 ± 0.66	18 ± 9
6	17:45:41.17	-29.0.17.84	67.20 ± 3.64	20.85 ± 0.34	12.92 ± 0.81	29 ± 10
7	17:45:41.03	-29.0.14.25	75.74 ± 2.80	38.98 ± 0.26	14.66 ± 0.63	31 ± 12
8	17:45:40.83	-29.0.12.78	48.81 ± 2.80	39.96 ± 0.44	15.65 ± 1.05	31 ± 13
9	17:45:40.03	-29.0.12.87	62.31 ± 2.53	77.80 ± 0.38	19.44 ± 0.93	40 ± 17
10	17:45:40.31	-29.0.43.77	71.32 ± 2.75	-42.98 ± 0.39	21.02 ± 0.95	56 ± 18
11	17:45:39.51	-29.0.36.96	50.43 ± 1.81	136.16 ± 0.96	55.51 ± 2.43	147 ± 39

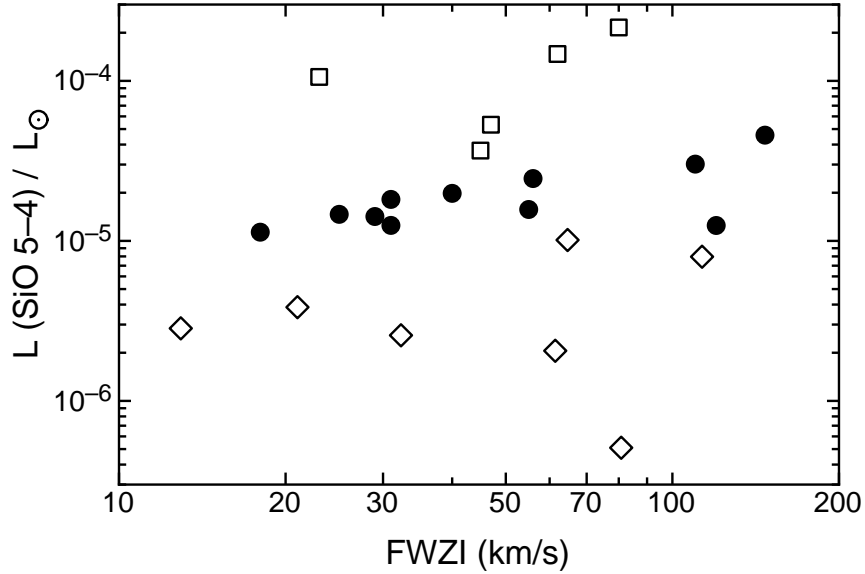


Fig. 4.— Filled circles show the luminosity in the SiO(5-4) line versus full line width (FWZI) for the 11 sources detected in the circumnuclear ring. Open diamonds and open squares show the corresponding quantities for outflows from low-mass YSOs (Gibb *et al.* 2004) and high-mass YSOs (Gibb *et al.* 2007), respectively.